

Probability density function/Monte Carlo simulation of near-wall turbulent flows

By THOMAS D. DREEBEN [†] AND STEPHEN B. POPE

Department of Mechanical and Aerospace Engineering, Cornell University, Ithaca,
NY 14853, USA.

(Received 11 January 1997 and in revised form 25 September 1997)

Probability density function (p.d.f.) methods are extended to include modelling of wall-bounded turbulent flows. A p.d.f. near-wall model is developed in which the generalized Langevin model is combined with a model for viscous transport. This provides exact treatment of viscous inhomogeneous effects, and enables consistent imposition of the no-slip condition in a particle framework. The method of elliptic relaxation is combined with additional boundary conditions and with the generalized Langevin model to provide an analogy for the near-wall fluctuating continuity equation. This provides adequate representation of the near-wall anisotropy of the Reynolds stresses. The model is implemented with a p.d.f./Monte Carlo simulation for the joint p.d.f. of velocity and turbulent frequency. Results are compared with DNS and experimental profiles for fully developed turbulent channel flow.

1. Introduction

In an effort to offer a more comprehensive approach for the modelling of turbulent reactive flows, probability density function (p.d.f.) methods are extended to include the modelling of near-wall flows. Many formulations to incorporate the effects of the wall in turbulence models involve the use of wall functions (Launder & Spalding 1974; Singhal & Spalding 1981; Rodi 1980; Spalding 1977; Dreeben & Pope 1997*b*), damping functions (Van Driest 1956; Lai & So 1990; So, Lai & Zhang 1991; Craft & Launder 1995; Shih & Lumley 1993; Hanjalic & Launder 1976; Launder & Tselepidakes 1991), or elliptic relaxation (Durbin 1991, 1993; Demuren & Wilson 1994; Laurence, Durbin & Demuren 1995; Dreeben & Pope 1997*a*). The model developed here uses the no-slip condition on velocity at the wall, and has no explicit dependence on wall-normal distance in the governing equations. In general, this can be achieved only with elliptic relaxation or with some of the damping-function methods (see for example, Craft & Launder 1995); our approach is to use elliptic relaxation in conjunction with the generalized Langevin model of Haworth & Pope (1986, 1987).

Much of this work is an extension of the modelling in Dreeben & Pope (1997*a*). That model combines a p.d.f./particle development with an Eulerian model for the dissipation, and demonstrates the computational feasibility of a derived Reynolds-stress closure. The current work combines the particle velocity model of Dreeben & Pope (1997*a*) with the stochastic turbulent frequency model of Jayesh & Pope (1995). Here, the model is implemented in a full p.d.f./Monte Carlo simulation.

[†] Present address: Combustion Research Facility, Sandia National Laboratories, Livermore, CA 94551-0969, USA.

We describe the modelling issues associated with bringing the p.d.f. method from its current state to the ability to characterize near-wall flows through the viscous sublayer. In §2, we define relevant terms and describe the common current implementation of p.d.f. methods without efforts to model the effects of the wall. The bulk of the paper is devoted to confronting the two main physical effects which are important in near-wall turbulence modelling: steep inhomogeneity and strong anisotropy in the viscous sublayer. Section 3 addresses inhomogeneity and includes a discussion of the no-slip condition on a particle level, plus modifications to the basic model which make the no-slip condition feasible to impose. Section 4 addresses the issue of modelling the near-wall anisotropy. A p.d.f. model emerges in §4 which is based on the one which appears in Dreeben & Pope (1997a), and is used to generate model profiles of turbulent statistics for fully developed channel flow. These results are shown with DNS and experimental data in §5. Relevant numerical issues which arise with the Monte Carlo method are discussed in the Appendix.

2. Current use of p.d.f. methods

To see what modifications the p.d.f. approach needs to handle near-wall flows, we briefly review a common high-Reynolds-number p.d.f. implementation which does not incorporate a solid wall. Let $\hat{f}(\mathbf{V}; \mathbf{x}, t)$ be the Eulerian p.d.f. of velocity \mathbf{U} at a given location \mathbf{x} . While turbulent moment closures aim to solve equations for moments of \hat{f} , a p.d.f. model forms a closure for \hat{f} itself. For density ρ , kinematic viscosity ν , and pressure decomposed into its mean and fluctuating components

$$\mathcal{P} = \langle \mathcal{P} \rangle + p, \quad (2.1)$$

Pope (1985) shows that the exact evolution equation for \hat{f} is

$$\frac{\partial \hat{f}}{\partial t} + V_i \frac{\partial \hat{f}}{\partial x_i} = \frac{1}{\rho} \frac{\partial \langle \mathcal{P} \rangle}{\partial x_i} \frac{\partial \hat{f}}{\partial V_i} + \frac{\partial}{\partial V_i} \left[\hat{f} \left\langle \frac{1}{\rho} \frac{\partial p}{\partial x_i} - \nu \frac{\partial^2 U_i}{\partial x_j \partial x_j} \right| \mathbf{U}(\mathbf{x}, t) = \mathbf{V} \right]. \quad (2.2)$$

We cannot solve (2.2) directly for \hat{f} because the right-hand side of the equation contains unknown terms in the form of conditional expectations. Instead, we construct a model whose domain is a field of probability densities of velocity, not of velocity itself. For time-scale information, we also include a stochastic characteristic frequency ω with sample space variable Ω . This leads to a closed equation for p.d.f. $f(\mathbf{V}, \Omega; \mathbf{x}, t)$ which we use as a model for \hat{f} . The model is based on an ensemble of particles: the general particle has position $\mathcal{X}(t)$ and velocity $\mathcal{U}(t)$. For infinitesimal time increment dt , each particle's position evolves like that of a fluid particle:

$$d\mathcal{X}_i = \mathcal{U}_i dt. \quad (2.3)$$

This equation is inherent to the Lagrangian approach of p.d.f. methods; it says that particles are to be convected through the domain, and it causes the associated processes of turbulent production, transport, and mean convection to appear in the governing equations in closed form.

The particle velocity evolves with a model for the terms

$$-\frac{1}{\rho} \frac{\partial \mathcal{P}}{\partial x_i} + \nu \frac{\partial^2 U_i}{\partial x_j \partial x_j} \quad (2.4)$$

in the Navier–Stokes equations. For

$$\langle U_i \rangle = \int V_i f \, dV \, d\Omega, \quad (2.5)$$

$$\langle u_i u_j \rangle = \int (V_i - \langle U_i \rangle) (V_j - \langle U_j \rangle) f \, dV \, d\Omega, \quad (2.6)$$

and model constant C_0 , the generalized Langevin model of Haworth & Pope (1986) specifies

$$d\mathcal{U}_i = -\frac{1}{\rho} \frac{\partial \langle \mathcal{P} \rangle}{\partial x_i} dt + G_{ij} (\mathcal{U}_j - \langle U_j \rangle) dt + (C_0 \epsilon)^{1/2} dW'_i, \quad (2.7)$$

where ϵ is the dissipation rate. The term dW'_i is an increment of the isotropic Wiener process \mathbf{W}' , in which each increment is a random variable with a normal $(0, dt)$ distribution and with

$$dW'_i dW'_j = dt \delta_{ij}. \quad (2.8)$$

The tensor G_{ij} is a function of $\partial \langle U_i \rangle / \partial x_j$, $\langle u_i u_j \rangle$, and ϵ . Considerable flexibility exists in how G_{ij} can be specified, depending on what sort of flow is to be modelled. Pope (1993b) has demonstrated how different choices of G_{ij} and C_0 make the generalized Langevin model equivalent to some of the well-known Reynolds-stress models such as Rotta's (1951) model and the IP (isotropization of production) model of Naot, Shavit & Wolfshtein (1970) and Launder, Reece & Rodi (1975). We begin with the simplified Langevin model of Pope (1993b) for G_{ij} :

$$G_{ij} = -\left(\frac{1}{2} + \frac{3}{4}C_0\right) \frac{\epsilon}{k} \delta_{ij}, \quad (2.9)$$

where

$$k = \frac{\langle u_i u_i \rangle}{2} \quad (2.10)$$

is the turbulent kinetic energy.

Like any turbulence model, p.d.f. ones need to carry some piece of time-scale information from which to determine ϵ . With traditional moment closures, the most common approach for this is to incorporate a modelled evolution equation for ϵ itself as in Daly & Harlow (1970). An alternative method due to Wilcox (1993) is to use an equation for a mean characteristic turbulent frequency $\langle \omega \rangle$, and then to define

$$\epsilon = k \langle \omega \rangle. \quad (2.11)$$

In recent years, p.d.f. methods have incorporated a stochastic model for turbulent frequency ω , developed by Pope & Chen (1990), Pope (1991), and Jayesh & Pope (1995). While it is a long-term goal to formulate a broadly applicable model for turbulent frequency, the model currently appears in different contexts with somewhat different forms. It has been used by Pope (1991) for free shear flows, by Norris & Pope (1995) and Saxena & Pope (1996) for combustion of a piloted jet diffusion flame, by Subramaniam & Pope (1997) for a periodic reaction zone model problem, by Delarue & Pope (1997) for compressible turbulent reacting flows, and by Van Slooten, Jayesh & Pope (1997) for a velocity/wave-vector p.d.f. model. For

$$\langle \omega \rangle = \int \Omega f \, dV \, d\Omega, \quad (2.12)$$

and ϵ given by (2.11), the simplest formulation of this frequency model is

$$d\omega = -C_3 \langle \omega \rangle (\omega - \langle \omega \rangle) dt - S_\omega \langle \omega \rangle \omega dt + (2C_3 C_4 \langle \omega \rangle^2 \omega)^{1/2} dW'' \quad (2.13)$$

Here, dW'' is another Wiener process, independent of dW'_i of (2.7). Model constant C_3 controls the statistical dependence of ω on the other particle properties, and C_4 controls the variance of the marginal p.d.f. of ω . The term involving S_ω accounts for generation and loss of mean turbulent frequency. Particle equations (2.3), (2.7), and (2.13) lead to evolution equations for $\langle U_i \rangle$, $\langle u_i u_j \rangle$, and $\langle \omega \rangle$ (Pope 1991; Dreeben & Pope 1997b). This provides a basic p.d.f. modelling framework from which to build a near-wall modelling capability.

3. Inhomogeneity: enabling use of the no-slip condition

In the viscous sublayer, near-wall turbulent flows are strongly inhomogeneous. For any turbulent statistic ϕ , this inhomogeneity is associated with the viscous transport term $\nu \nabla^2 \phi$ appearing in the governing equations for ϕ as a dominant term close to the wall. If f is the p.d.f. of all relevant field properties, the viscous transport terms correspond to a term $\nu \nabla^2 f$ in the p.d.f. evolution equation. For the p.d.f. model described above, there is no explicit representation of viscosity. Beyond the issue of inhomogeneity, the neglect of the viscous terms poses a difficulty with self-consistency at the wall. Physically, the viscous term $\nu \nabla^2 \langle U_j \rangle$ balances the mean pressure gradient in the mean velocity equation close to the wall. In a model without the viscous term, the no-slip condition forces the mean pressure gradient to zero at the wall. This contradicts the condition of any pressure-driven flow such as pipe flow, in which the streamwise pressure gradient is non-zero all the way to the wall. So the viscous effects need to appear in the model for self-consistency as well as modelling accuracy. The aim of this section is to incorporate the viscous transport terms and the wall boundary condition into the model of §2.

3.1. From fluid particles to stochastic particles

For inhomogeneous turbulent flows, we know from Pope (1985) that (2.2) can be written as

$$\begin{aligned} \frac{\partial \hat{f}}{\partial t} + V_i \frac{\partial \hat{f}}{\partial x_i} &= \nu \frac{\partial^2 \hat{f}}{\partial x_i \partial x_i} + \frac{1}{\rho} \frac{\partial \langle \mathcal{P} \rangle}{\partial x_i} \frac{\partial \hat{f}}{\partial V_i} - \frac{\partial^2}{\partial V_i \partial V_j} \\ &\times \left[\hat{f} \left\langle \nu \frac{\partial U_i}{\partial x_k} \frac{\partial U_j}{\partial x_k} \middle| \mathbf{U}(\mathbf{x}, t) = \mathbf{V} \right\rangle \right] + \frac{\partial}{\partial V_i} \left[\hat{f} \left\langle \frac{1}{\rho} \frac{\partial p}{\partial x_i} \middle| \mathbf{U}(\mathbf{x}, t) = \mathbf{V} \right\rangle \right], \end{aligned} \quad (3.1)$$

where the viscous transport appears as the first term on the right-hand side. The model of §2 must be modified in a way which includes this term in the p.d.f. evolution equation. Because the term involves a diffusion of the p.d.f. in physical space (as opposed to velocity space), it can only appear through a modification of the evolution of particle position, (2.3). The diffusion is best represented by Brownian motion, described by Einstein (1926). Accordingly, we specify the particle position to be

$$d\mathbf{x}_i = \mathcal{U}_i dt + (2\nu)^{1/2} dW_i. \quad (3.2)$$

With this equation, the particles carry momentum with them in the same way that molecules do, and with the same statistical properties. Woelfert (1995) has used this method in near-wall modelling, and Colucci *et al.* (1998) have used it for variable-property mixing in the context of reacting flows.

Two important consequences follow from (3.2). First, the particle trajectories are no longer differentiable functions of time: they cannot be envisioned as fluid particles or material points. We refer to them as stochastic particles, and their motion is chosen to bring out an aspect of the flow which is crucial to near-wall modelling: viscous transport. But it should be noted that the velocity information of the model is embodied in the *particle property* \mathcal{U} , not in the particle motion.

The second consequence of (3.2) is that (2.7) must be modified for consistency with the additional random motion. Dreeben & Pope (1997a) develop this modification and its associated particle velocity equation:

$$d\mathcal{U}_i = -\frac{1}{\rho} \frac{\partial \langle \mathcal{P} \rangle}{\partial x_i} dt + 2\nu \frac{\partial^2 \langle U_i \rangle}{\partial x_j \partial x_j} dt + (2\nu)^{1/2} \frac{\partial \langle U_i \rangle}{\partial x_j} dW_j + G_{ij} (\mathcal{U}_j - \langle U_j \rangle) dt + (C_0 \epsilon)^{1/2} dW'_i. \quad (3.3)$$

Note that the Wiener process on the first line of (3.3) is identical to the one of (3.2).

For laminar flow, the p.d.f. of velocity is a delta function, and the mean velocity at a given location is just the particle velocity at that location. In this case, (3.2) and the first line of (3.3) form a Monte Carlo formulation for the Navier–Stokes equations.

For turbulent flow, (3.2), (3.3), and (2.13) lead to the new p.d.f. equation:

$$\begin{aligned} \frac{\partial f}{\partial t} + V_i \frac{\partial f}{\partial x_i} = & \nu \frac{\partial^2 f}{\partial x_i \partial x_i} + \frac{\partial f}{\partial V_i} \frac{1}{\rho} \frac{\partial \langle \mathcal{P} \rangle}{\partial x_i} - \frac{\partial}{\partial V_i} [G_{ij} (V_j - \langle U_j \rangle) f] \\ & + 2\nu \frac{\partial \langle U_j \rangle}{\partial x_i} \frac{\partial^2 f}{\partial x_i \partial V_j} + \nu \frac{\partial \langle U_i \rangle}{\partial x_k} \frac{\partial \langle U_j \rangle}{\partial x_k} \frac{\partial^2 f}{\partial V_i \partial V_j} + \frac{1}{2} C_0 \epsilon \frac{\partial^2 f}{\partial V_i \partial V_i} \\ & + C_3 \langle \omega \rangle \frac{\partial}{\partial \Omega} [(\Omega - \langle \omega \rangle) f] + S_\omega \langle \omega \rangle \frac{\partial}{\partial \Omega} (\Omega f) + C_3 C_4 \langle \omega \rangle^2 \frac{\partial^2 (\Omega f)}{\partial \Omega \partial \Omega}. \end{aligned} \quad (3.4)$$

For the incompressible flow considered here, the steps for deriving an Eulerian p.d.f. equation such as (3.4) from particle equations are described in Dreeben & Pope (1997a), and further depth is provided in Pope (1985), Wax (1954), and Dreeben (1996). Governing equations for any statistic ϕ are determined by multiplying (3.4) by the sample space variable associated with ϕ and then integrating over velocity and frequency space. Dreeben (1996) provides detailed calculation of these moment equations. For

$$\frac{\tilde{D}(\cdot)}{Dt} = \frac{\partial(\cdot)}{\partial t} + \langle U_k \rangle \frac{\partial(\cdot)}{\partial x_k}, \quad (3.5)$$

the modelled governing equations for $\langle U_i \rangle$, $\langle u_i u_j \rangle$, and $\langle \omega \rangle$ are

$$\frac{\tilde{D} \langle U_j \rangle}{Dt} = -\frac{1}{\rho} \frac{\partial \langle \mathcal{P} \rangle}{\partial x_j} - \frac{\partial}{\partial x_i} \langle u_i u_j \rangle + \nu \frac{\partial^2 \langle U_j \rangle}{\partial x_i \partial x_i}, \quad (3.6)$$

$$\begin{aligned} \frac{\tilde{D} \langle u_i u_j \rangle}{Dt} = & \nu \frac{\partial^2 \langle u_i u_j \rangle}{\partial x_k \partial x_k} - \frac{\partial \langle u_i u_j u_k \rangle}{\partial x_k} - \left(\langle u_i u_k \rangle \frac{\partial \langle U_j \rangle}{\partial x_k} + \langle u_j u_k \rangle \frac{\partial \langle U_i \rangle}{\partial x_k} \right) \\ & + G_{ik} \langle u_k u_j \rangle + G_{jk} \langle u_k u_i \rangle + C_0 \epsilon \delta_{ij}, \end{aligned} \quad (3.7)$$

$$\frac{\tilde{D} \langle \omega \rangle}{Dt} = \nu \frac{\partial^2 \langle \omega \rangle}{\partial x_i \partial x_i} - \frac{\partial \langle u_i \omega \rangle}{\partial x_i} - S_\omega \langle \omega \rangle^2. \quad (3.8)$$

The inclusion of Brownian motion in (3.2) leads to the important $\nu \nabla^2 f$ term on the right-hand side of (3.4). This in turn leads to the viscous transport terms in the

moment equations. The Laplacian term of (3.6) allows self-consistent implementation of the no-slip condition at the wall, and the Laplacian term of (3.7) permits accurate representation of the dominant near-wall balances of the Reynolds stresses (Dreeben & Pope 1997a).

The no-slip condition also requires a modification to the definition of ϵ . Equation (2.11) is appropriate for high-Reynolds-number flows, but it incorrectly forces ϵ to zero at the wall, when physically ϵ reaches a non-zero peak there. An appropriate definition of ϵ allows Kolmogorov scaling close to the wall, and the scaling of (2.11) far from the wall. Accordingly, we assign

$$\epsilon = \langle \omega \rangle (k + \nu C_T^2 \langle \omega \rangle). \quad (3.9)$$

The model constant C_T is chosen so that in the limit as $k \rightarrow 0$ (3.9) is equivalent to the scaling of the time scale T of Durbin (1993) and with the identical value of $C_T = 6.0$.

3.2. Wall boundary conditions on particles

Particle boundary conditions amount to specification of the joint p.d.f. of velocity and ω at the wall for the p.d.f. equation (3.4). They must also be consistent with the physical boundary conditions which are known to apply to the partial differential equations (3.6), (3.7), and (3.8).

3.2.1. Treatment of particle position

The wall boundary condition on particle properties depends on our ability to distinguish those particles which strike the wall (taken to be $y = x_2 = 0$) from those which do not (Pope 1993a). The location of each particle is governed by (3.2). For flow in the viscous sublayer, the local fluid velocity \mathcal{U} is sufficiently small compared to the stochastic term that the particle's distance from the wall \mathcal{Y} is governed by Brownian motion with

$$d\mathcal{Y} = (2\nu)^{1/2} dW_2. \quad (3.10)$$

So the appropriate model for the particle location in the region adjacent to the wall is reflected Brownian motion in which

$$\mathcal{Y}(t + dt) = |\hat{\mathcal{Y}}(t + dt)|, \quad (3.11)$$

where $\hat{\mathcal{Y}}(t + dt) = \mathcal{Y}(t) + d\mathcal{Y}$. Over any given time interval, a particle undergoing reflected Brownian motion can strike the wall infinitely many times. For a particle located at y_0 at time $t = 0$, we consider its non-reflected motion over a small finite time step Δt , and then keep track of which particles have struck the wall and which have not. Each particle can have trajectories of three different types, shown in figure 1. Trajectory 1 crosses the wall and becomes negative at the end of the time step, trajectory 2 crosses the wall and returns to become positive, and trajectory 3 remains positive without ever touching the wall. Given only the particle's location at the beginning and the end of the time step, the boundary condition must impose no slip and impermeability for trajectories 1 and 2, but not for trajectory 3. For each particle, (3.10) distinguishes trajectory 1 from the other two. If

$$\hat{\mathcal{Y}}(t + \Delta t) = y_b < 0, \quad (3.12)$$

then the particle undergoing reflected Brownian motion has clearly struck the wall; the particle properties are reset according to the specifications which follow in § 3.2.2,

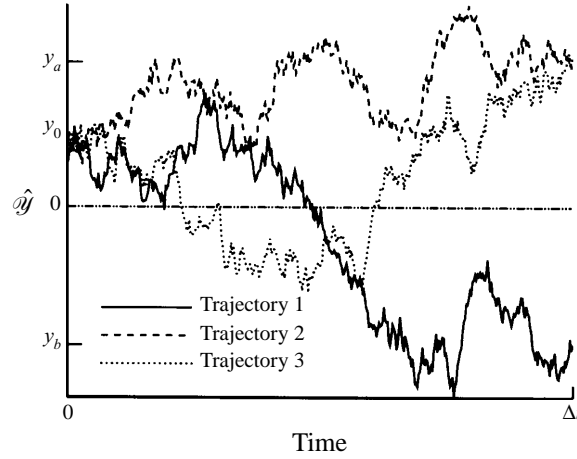


FIGURE 1. Possible non-reflective trajectories of a particle from a point in the viscous sublayer of the computational domain.

and the new location of the particle is $|y_b|$. But if (3.10) gives

$$\hat{\mathcal{Y}}(t + \Delta t) = y_a > 0, \quad (3.13)$$

then the particle may take trajectory 2 or trajectory 3 to get there, and only trajectory 3 involves contact with the wall. The likelihood of trajectory 3 (and hence of the need to reset particle properties) is just the probability that the particle strikes the wall over time step Δt given that it begins at y_0 and ends at y_a . If $m_{\Delta t}$ is the running minimum of y over the interval Δt , then standard methods described by Karatzas & Shreve (1991) can be used to show that

$$P[m_{\Delta t} < 0 | \mathcal{Y}(0) = y_0, \mathcal{Y}(\Delta t) = y_a] = \exp\left[\frac{-y_0 y_a}{v \Delta t}\right]. \quad (3.14)$$

To implement these ideas numerically, we specify the particle's position after Δt

$$\underline{\mathcal{X}}(t + \Delta t) = (x_1, y_1, z_1), \quad (3.15)$$

given its initial position

$$\underline{\mathcal{X}}(t) = (x_0, y_0, z_0). \quad (3.16)$$

Based on (3.2), we set

$$\hat{x}_1 = x_0 + \mathcal{U} \Delta t + (2v \Delta t)^{1/2} \xi, \quad (3.17)$$

$$\hat{y}_1 = y_0 + \mathcal{V} \Delta t + (2v \Delta t)^{1/2} \xi', \quad (3.18)$$

$$\hat{z}_1 = z_0 + \mathcal{W} \Delta t + (2v \Delta t)^{1/2} \xi'', \quad (3.19)$$

where the ξ are independent standard Gaussian random variables. Then the new location is

$$x_1 = \hat{x}_1, \quad (3.20)$$

$$y_1 = |\hat{y}_1|, \quad (3.21)$$

$$z_1 = \hat{z}_1. \quad (3.22)$$

The particle properties of velocity and ω are reset according to the specifications

described in §3.2.2 if

$$\{\hat{y}_1 < 0\} \text{ (trajectory 1),} \quad (3.23)$$

or if

$$\left\{ \hat{y}_1 \geq 0 \text{ and } \exp \left[\frac{-y_0 y_a}{v \Delta t} \right] > \eta \right\} \text{ (trajectory 3),} \quad (3.24)$$

where η is a random variable with a standard uniform distribution. Otherwise (trajectory 2), the particle properties are not reset.

3.2.2. Particle boundary specifications

The task of the particle boundary condition is to impose no-slip and impermeability on the velocities, and to choose a statistical behaviour of ω which ensures that the model produces the correct near-wall balance in the kinetic energy equation:

$$vk'' - \epsilon = 0, \quad (3.25)$$

where the $'$ superscript denotes a derivative in the wall-normal direction.

The condition on velocities is straightforward: for those particles which strike the wall, we set

$$\mathcal{U}_i(t + \Delta t) = 0. \quad (3.26)$$

For ω , we see that the specification

$$\langle \omega \rangle = \frac{[k''(0)]^{1/2}}{C_T} \quad (3.27)$$

imposes (3.25) through the model definition of ϵ in (3.9). If we assume that $k(0) = k'(0) = 0$, then (3.27) can be expressed in a way that is easier to compute accurately:

$$\langle \omega \rangle = \frac{[(2k)^{1/2}]'}{C_T}. \quad (3.28)$$

The condition on the distribution of ω is based on the work of Jayesh & Pope (1995). A gamma distribution is given for those particles which strike the wall, with its mean $\langle \omega \rangle$ specified by (3.28). It is found that the near-wall values of $\langle \omega \rangle$ and ϵ are insensitive to the variance of the distribution of ω at the wall. The variance of ω is set to

$$C_4 \langle \omega \rangle^2, \quad (3.29)$$

which is the variance of ω for the stationary solution of a simplified (2.13), in which the sink term in S_ω has been removed. At the wall, the joint p.d.f. of velocity and frequency is a delta function about $\mathcal{U}_i = 0$ for the velocities with a gamma distribution for the turbulent frequency.

3.3. A local model with the no-slip condition

Here we assemble a Monte Carlo simulation for a model with the no-slip boundary condition and with the viscous transport terms described above. This is partly to demonstrate the computational feasibility of the no-slip condition in a particle framework, and partly to set the stage for the further developments of the model in §4. The model which follows is nearly equivalent to including the viscous terms and the no-slip condition in Rotta's model. The term 'local' is used to distinguish it from the non-local model which appears in §4.

The particle equations to be used are (3.2), (3.3), and (2.13), with G_{ij} specified by (2.9). Model constants here are set to previously established values, although

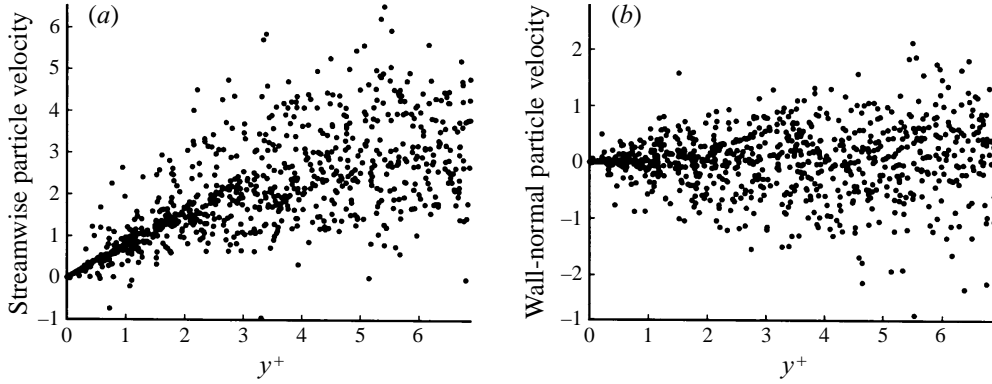


FIGURE 2. (a) Streamwise and (b) wall-normal particle velocities for the local model.

refinement of the model in the light of available direct numerical simulation (DNS) data leads to some modifications of these constants in §4. The model constant C_0 was originally meant to be universal in accordance with the theory of Kolmogorov (1941), and was chosen by Pope (1985) to be $C_0 = 2.1$. However, Pope (1994a) notes that values of C_0 closer to 5.0 have been observed and inferred from numerical simulations. We adopt the value $C_0 = 3.5$ which is used successfully for inhomogeneous flows by Pope & Chen (1990).

The term S_ω in (2.13) is given by Pope & Chen (1990) as

$$S_\omega = C_{\omega 2} - C_{\omega 1} \frac{P}{\epsilon} \quad (3.30)$$

where

$$P = -\langle u_i u_j \rangle \frac{\partial \langle U_i \rangle}{\partial x_j} \quad (3.31)$$

is the production of turbulent kinetic energy and $C_{\omega 1}$ and $C_{\omega 2}$ are model constants. Like the ϵ equation in k - ϵ type closures, (3.8) contains transport (first two terms on the right-hand side), a source and a sink. For homogeneous flows, Pope & Chen (1990) show that the source and sink of ω embodied in (3.30) are related to the corresponding terms of the ϵ equation by

$$C_{\omega 1} = C_{\epsilon 1} - 1, \quad (3.32)$$

$$C_{\omega 2} = C_{\epsilon 2} - 1. \quad (3.33)$$

Based on common values from the k - ϵ model, plausible values of the constants in S_ω are $C_{\omega 1} = 0.44$ and $C_{\omega 2} = 0.9$. The constant $C_3 = 5.0$ of (2.13) controls the turbulent transport term of (3.8). It is chosen to be consistent with a p.d.f. constant-stress layer analysis of Dreeben & Pope (1997b), which sets the von Kármán constant $\kappa = 0.41$ for the model of §2. The constant $C_4 = 0.25$ is the same one used by Jayesh & Pope (1995) which was originally chosen to match DNS results of Yeung & Pope (1989) for isotropic turbulence.

Using the Fortran code of Pope (1994b), a Monte Carlo simulation is implemented with the local model and boundary conditions described here for fully developed channel flow at Reynolds number

$$Re_\tau = \frac{u_* L}{\nu} = 395, \quad (3.34)$$

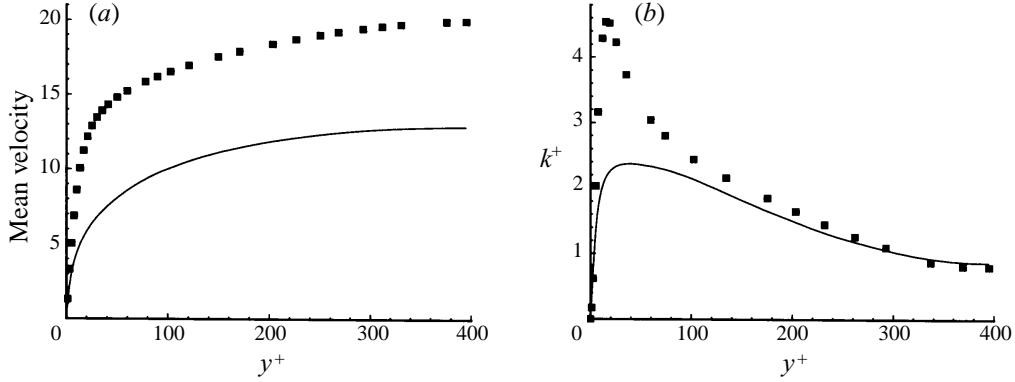


FIGURE 3. (a) Mean velocity and (b) kinetic energy: local model (line) and DNS data (symbols) for fully developed channel flow.

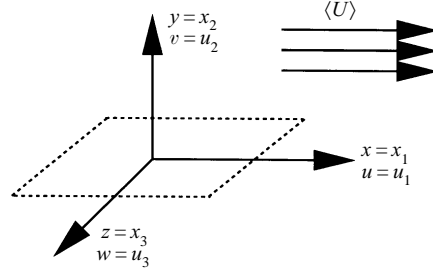


FIGURE 4. Coordinate system relative to the wall and the mean flow.

where u_* is the friction velocity and L is the channel half-width. Figures 2(a) and 2(b) are scatter plots of the streamwise and wall-normal components of particle velocity, shown from the wall to $y^+ = 6$. All velocities shown are normalized by u_* . These results show successful use of the no-slip and impermeability conditions. Mean velocity and turbulent kinetic energy for the local model are shown together with DNS results of N. N. Mansour (private communication) in figures 3(a) and 3(b). While these results show that the particle boundary conditions work properly, it is clear that the model as it stands is inadequate. Although the inhomogeneous terms for velocity and Reynolds stress all appear in closed form in (3.6) and (3.7), the important issue of near-wall anisotropy needs to be addressed.

4. Anisotropy

4.1. Why we need to model anisotropy close to the wall

The results of the local model are used to bring out the important role of anisotropy and near-wall scaling of the Reynolds stresses in constructing the model. For a coordinate system arranged as in figure 4, it seems clear from figure 3(a) that close to the wall, the Reynolds shear stress $-\langle uv \rangle$ given by the local model is too high. Figure 5 shows this shear stress: while the agreement with DNS is quite close over the bulk of the domain, the strong overprediction of $-\langle uv \rangle$ within $y^+ = 26$ appears to be sufficient to send the velocity profile awry.

An important feature of near-wall turbulence is that those Reynolds stresses with a normal component scale with powers of y higher than 2. Mansour, Kim & Moin

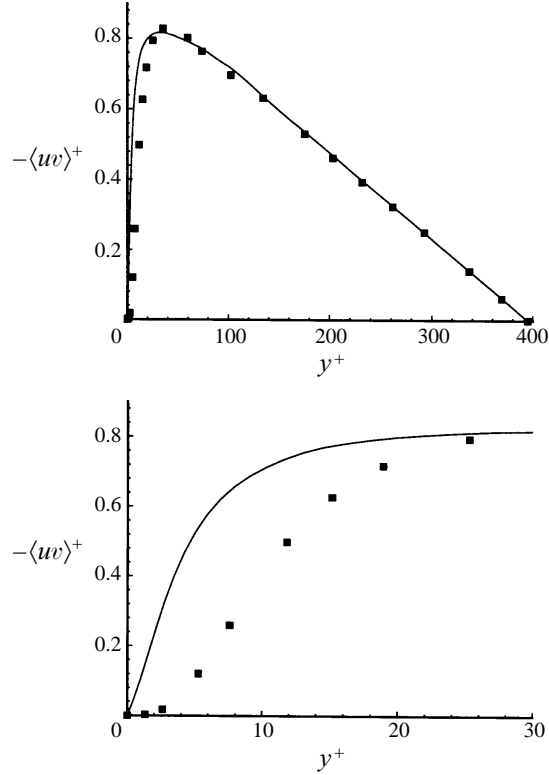


FIGURE 5. Reynolds shear stress: local model (line) and DNS data (symbols) for fully developed channel flow.

(1988) have shown that this is a consequence of the fluctuating continuity equation very close to the wall, which makes v' scale with y^2 rather than y . Durbin (1991) has shown that this suppression of v' in the viscous sublayer is important for near-wall turbulence models. In particular, the physical scaling of the Reynolds stresses is

$$\langle u^2 \rangle \sim y^2, \quad (4.1)$$

$$\langle v^2 \rangle \sim y^4, \quad (4.2)$$

$$\langle w^2 \rangle \sim y^2, \quad (4.3)$$

$$\langle uv \rangle \sim y^3. \quad (4.4)$$

The near-wall anisotropy arises because those components of Reynolds stress which are purely parallel to the wall (in this case $\langle u^2 \rangle$ and $\langle w^2 \rangle$) dominate the other components. The local model is unable to capture this anisotropy because the simple Langevin model of (2.9) allows no inherent distinction between the behaviours of \mathcal{U} , \mathcal{V} , and \mathcal{W} close to the wall, so that turbulent intensities in one direction cannot dominate intensities in another. Figure 6 shows the model and the DNS data on Lumley's (1978) anisotropy map. At the wall, the true Reynolds stresses reach their two-component limit which is represented by the top line of the triangle. Clearly the local model never comes close to that limit, since all Reynolds stresses are of comparable magnitude throughout the domain.

Most near-wall turbulence models incorporate a near-wall suppression of v' relative to u' and w' in the Reynolds stresses to achieve a plausible velocity profile. A common

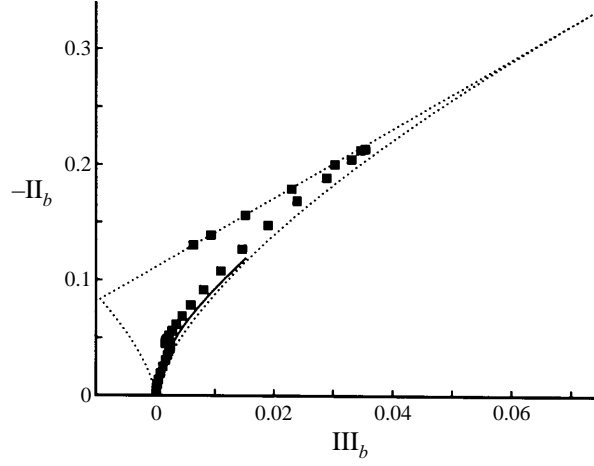


FIGURE 6. Anisotropy map: local model (line) and DNS data (symbols) for fully developed channel flow.

approach is to connect an asymptotically correct (or nearly correct) local model for the viscous sublayer with a relatively isotropic model far from the wall, using a damping function (Hanjalic & Launder 1976; So *et al.* 1991; Lai & So 1990; Craft & Launder 1995; Launder & Tselepidakes 1991). An alternative approach (Durbin 1991, 1993) which is followed here involves a non-local model using elliptic relaxation. This has been used by others (Demuren & Wilson 1994; Laurence *et al.* 1995), and has been incorporated into the generalized Langevin model as a Reynolds-stress closure by Dreeben & Pope (1997a).

4.2. Elliptic relaxation

To model the near-wall anisotropy effectively, elliptic relaxation is used in conjunction with additional boundary conditions to provide a particle model for the effect of the fluctuating continuity equation close to the wall. The primary modification to the local model of §3 is the specification of G_{ij} and C_0 , based on the model of Dreeben & Pope (1997a). We introduce a tensor \wp_{ij} to characterize the non-local effect of fluctuating pressure, and set

$$G_{ij} = \frac{\wp_{ij} - \frac{1}{2}\epsilon\delta_{ij}}{k}, \quad (4.5)$$

$$C_0 = \frac{-2\wp_{ij}\langle u_i u_j \rangle}{3k\epsilon}. \quad (4.6)$$

With vanishing k and non-zero ϵ at the wall, G_{ij} becomes negative without bound as $y \rightarrow 0$. This poses a numerical difficulty for the solution of (3.3), which is addressed in the Appendix, §A.1. To define \wp_{ij} we first define a length scale. Following Durbin (1993), we take the maximum of the turbulent and the Kolmogorov scales:

$$L = C_L \max \left[\frac{k^{3/2}}{\epsilon}, C_\eta \left(\frac{\nu^3}{\epsilon} \right)^{1/4} \right], \quad (4.7)$$

where C_L and C_η are model constants. Then we specify the non-local term \wp_{ij} with the following elliptic-relaxation equation:

$$\wp_{ij} - L\nabla^2 (L\wp_{ij}) = \frac{1 - C_1}{2} k \langle \omega \rangle \delta_{ij} + k H_{ijkl} \frac{\partial \langle U_k \rangle}{\partial x_l}, \quad (4.8)$$

where

$$H_{ijkl} = (C_2 A_v + \frac{1}{3} \gamma_5) \delta_{ik} \delta_{jl} - \frac{1}{3} \gamma_5 \delta_{il} \delta_{jk} + \gamma_5 b_{ik} \delta_{jl} - \gamma_5 b_{il} \delta_{jk}, \quad (4.9)$$

$$A_v = \min \left[1.0, C_v \frac{\det \langle u_i u_j \rangle}{(\frac{2}{3} k)^3} \right], \quad (4.10)$$

and

$$b_{ij} = \frac{\langle u_i u_j \rangle}{\langle u_k u_k \rangle} - \frac{1}{3} \delta_{ij} \quad (4.11)$$

is the Reynolds-stress anisotropy tensor. Close to the wall, the Laplacian term of (4.8) becomes important and the term \wp_{ij} depends on the turbulent statistics throughout the domain, by analogy with the fact that pressure has non-local dependence as well. Far from the wall, the Laplacian term becomes negligible and \wp_{ij} depends only on the local quantities in the forcing term on the right-hand side of (4.8). For sufficient distance from the wall, those terms form the Lagrangian equivalent (see Pope 1993b) of a modified IP model. The modification involves incorporating the term A_v in (4.9), in an effort to improve the model's performance in the logarithmic layer. The behaviour of the logarithmic profile is sensitive to the Reynolds-stress redistribution, which in turn is most sensitive to the IP model source term in question. Durbin (1991) has argued that in a $k-\epsilon$ type closure, the turbulent viscosity scales with the wall-normal turbulent intensity $\langle v^2 \rangle$ rather than with k , and hence is suppressed close to the wall. By analogy, this p.d.f. model captures the logarithmic layer more accurately when the IP source term is similarly suppressed near the wall. The term A_v is an invariant which behaves like $\langle v^2 \rangle / k$ close to the wall (for an appropriately chosen constant C_v). Far from the wall, we have $A_v = 1.0$, and the source term is identical to that of the standard IP model. This modification improves the behaviour of the mean velocity profile in the log layer, with the IP model constant $C_2 = 0.63$. The fact that C_2 is close to its original value of $C_2 = 0.6$ preserves the ability of the current model to characterize a sudden distortion of initially isotropic turbulence, as Launder *et al.* (1975) describe. Model constants are identical to those of Dreeben & Pope (1997a), except for C_1 which is slightly larger here:

$$C_1 = 1.85; C_2 = 0.63; C_v = 1.4; \gamma_5 = 0.1; C_T = 6.0; C_L = 0.134; C_\eta = 72.0. \quad (4.12)$$

Both C_1 and C_2 are very close to their original values from Launder *et al.* of $C_1 = 1.8$ and $C_2 = 0.6$. Although the above modelling alone is sufficient to produce a plausible velocity profile, near-wall scaling, and anisotropy, small modifications are needed to the equation for ω to improve the performance of the model in the wake region at the channel half-plane. We set

$$S_\omega = C_{\omega 2} - C_{\omega 1} \frac{P}{\epsilon} + C_5 \max \left(0, 1 - \frac{P}{\epsilon} \right)^3, \quad (4.13)$$

with

$$C_{\omega 1} = 0.44; C_{\omega 2} = 0.73; C_3 = 5.0; C_4 = 0.25; C_5 = 0.3. \quad (4.14)$$

The particle equations for the non-local model are identical to those of the local model, given by (3.2), (3.3), and (2.13).

4.3. Near-wall behaviour

Because of the Laplacian term in (4.8), the non-local parameter \wp_{ij} needs a boundary condition at the wall. It will be shown below that a suitable condition is

$$\wp_{ij} = -4.5 \epsilon n_i n_j. \quad (4.15)$$

To examine the near-wall behaviour of the model, we expand each Reynolds stress in a Taylor series about the wall, impose the boundary conditions on the particles and on \wp_{ij} , and impose the Reynolds-stress equation (3.7). The particle velocity equation reduces to

$$d\mathcal{U}_i = \frac{\wp^{(iii)} - \frac{1}{2}\epsilon}{k} (\mathcal{U}_i - \langle U_i \rangle) dt \quad (4.16)$$

where parentheses around the indices of \wp suppress the summation. This is a relaxation equation of particle velocity to its local mean value. Velocity fluctuations are suppressed to a degree that depends on the diagonal components of \wp_{ij} . Here, the boundary condition on \wp_{ij} is used to distinguish the effect of the Langevin model in different directions. By setting only the wall-normal component of \wp_{ij} to be non-zero and negative in (4.15), we suppress fluctuations in the wall-normal velocity relative to the other two components. This provides an analogy to the effect of the fluctuating continuity equation adjacent to the wall.

Without loss of generality, the near-wall scaling of Reynolds stresses and anisotropy are determined in the coordinate system of figure 4. The governing near-wall Reynolds-stress equations reduce to

$$v \frac{\partial^2 \langle u^2 \rangle}{\partial y^2} - \frac{\epsilon}{k} \langle u^2 \rangle = O(y), \quad (4.17)$$

$$v \frac{\partial^2 \langle v^2 \rangle}{\partial y^2} + \frac{\frac{4}{3}\wp_{22} - \epsilon}{k} \langle v^2 \rangle = O(y), \quad (4.18)$$

$$v \frac{\partial^2 \langle w^2 \rangle}{\partial y^2} - \frac{\epsilon}{k} \langle w^2 \rangle = O(y), \quad (4.19)$$

$$v \frac{\partial^2 \langle uv \rangle}{\partial y^2} + \frac{\wp_{22} - \epsilon}{k} \langle uv \rangle = O(y). \quad (4.20)$$

To see how the solutions of these behave, we simplify them using the near-wall scaling properties of k . Because $k \sim y^2$ close to the wall, (3.25) implies that to leading order,

$$\frac{\epsilon}{k} = \frac{2v}{y^2}. \quad (4.21)$$

If we substitute (4.21) into (4.17)–(4.20), then these equations all reduce to ordinary differential equations in y of the form

$$\langle u_i u_j \rangle'' - \alpha_{(ij)} \frac{\langle u_i u_j \rangle}{y^2} = O(y). \quad (4.22)$$

Again, parentheses around the indices i and j indicate that the summation is to be suppressed. The solution to (4.22) is the sum of the homogeneous solution (not to be confused with a solution for homogeneous *turbulence*) $\langle u_i u_j \rangle_h$ and the particular

solution $\langle u_i u_j \rangle_p$ where

$$\langle u_i u_j \rangle_h = A_{(ij)} y^{\{(1-[1+4\alpha_{(ij)}]^{1/2})/2\}} + B_{(ij)} y^{\{(1+[1+4\alpha_{(ij)}]^{1/2})/2\}}, \quad (4.23)$$

$$\langle u_i u_j \rangle_p = C_{(ij)} y^3. \quad (4.24)$$

The constants $A_{(ij)}$ and $B_{(ij)}$ reflect the two degrees of freedom associated with the second-order differential equation; $C_{(ij)}$ is determined by the $O(y)$ forcing term on the right-hand side of (4.22). For all combinations of i and j , the exponent of the first term of (4.23) is negative, so the no-slip boundary condition forces

$$A_{(ij)} = 0. \quad (4.25)$$

For each Reynolds stress, the near-wall scaling is determined by either the homogeneous term in $B_{(ij)}$ or by the particular term in $C_{(ij)}$. The term which scales with a lower power of y is the dominant term. For $\langle u^2 \rangle$ and $\langle w^2 \rangle$ in which all Reynolds-stress components are parallel to the wall, we have from (4.15), (4.17), (4.19), and (4.21) that

$$\alpha_{(11)} = \alpha_{(33)} = 2. \quad (4.26)$$

This implies through (4.23) that the homogeneous solutions of (4.22) scale with y^2 . So (compared to $\langle u_i u_j \rangle_p \sim y^3$) the homogeneous terms dominate the solutions and the model gives

$$\langle u^2 \rangle \sim \langle w^2 \rangle \sim k \sim y^2, \quad (4.27)$$

which is the correct physical behaviour of these components. For $\langle v^2 \rangle$, we find from (4.15), (4.18), and (4.21) that

$$\alpha_{(22)} = 14, \quad (4.28)$$

which makes the homogeneous solution of (4.22) scale with $y^{4.27}$. So for this case the particular solution dominates and we have

$$\langle v^2 \rangle \sim y^3. \quad (4.29)$$

For the case of Reynolds shear stress, the identical argument shows that

$$\langle uv \rangle \sim y^3. \quad (4.30)$$

Comparison of (4.27), (4.29), and (4.30) with (4.2)–(4.4) shows that the model correctly reproduces the near-wall scaling in all of the Reynolds stresses except for $\langle v^2 \rangle$. It is a common feature of elliptic relaxation models that the near-wall Reynolds stresses with a wall-normal component scale with the same power of y . In our case that power is 3; in others such as Durbin (1993) the power is 4. So of the two Reynolds-stresses $\langle uv \rangle$ and $\langle v^2 \rangle$, one is represented correctly and the other is off by one power of y . But the important point is that the suppression of v' causes the Reynolds-stress components which are parallel to the wall to dominate those with a normal component as the wall is approached. In that limit, we expect the anisotropy to approach its two-component state. Particle wall boundary conditions are given by (3.26), (3.28), and (3.29), for those particles which strike the wall according to (3.23) and (3.24). The boundary condition on ϕ_{ij} is given by (4.15).

Here is a synopsis of the complete model. The particle properties of position, velocity, and turbulent frequency are governed by (3.2), (3.3), (2.13) respectively. Dissipation is given by (3.9). The model terms G_{ij} , C_0 , and S_ω are given by (4.5)–(4.14).

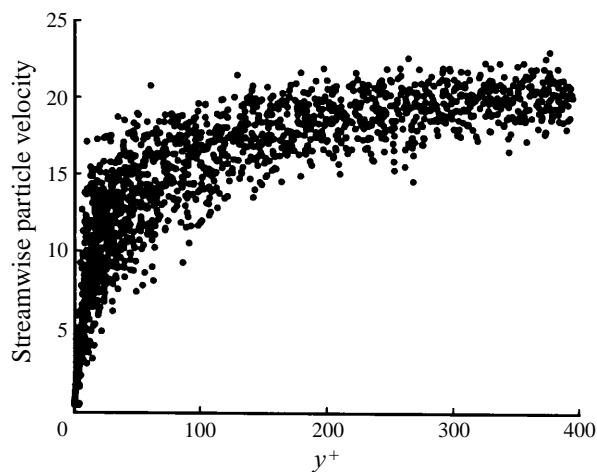


FIGURE 7. Streamwise particle velocities for the non-local model.

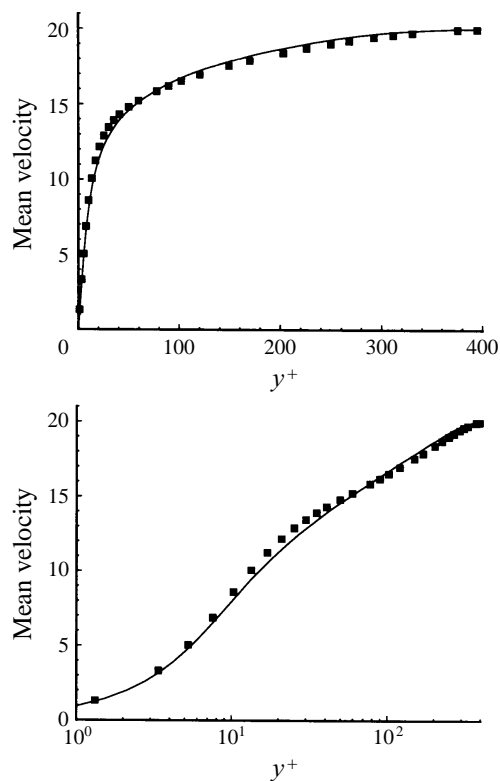


FIGURE 8. Mean velocity: non-local model (line) and DNS data (symbols) for fully developed channel flow.

5. Results for fully developed channel flow

The model is implemented using a Monte Carlo simulation of Pope (1994*b*), adapted to fully developed channel flow with $Re_\tau = 395$, based on the friction velocity and the channel half-width. The equations are solved on a 60 cell grid, with 480 particles per cell. Grid-independent solutions are obtained to the extent that the

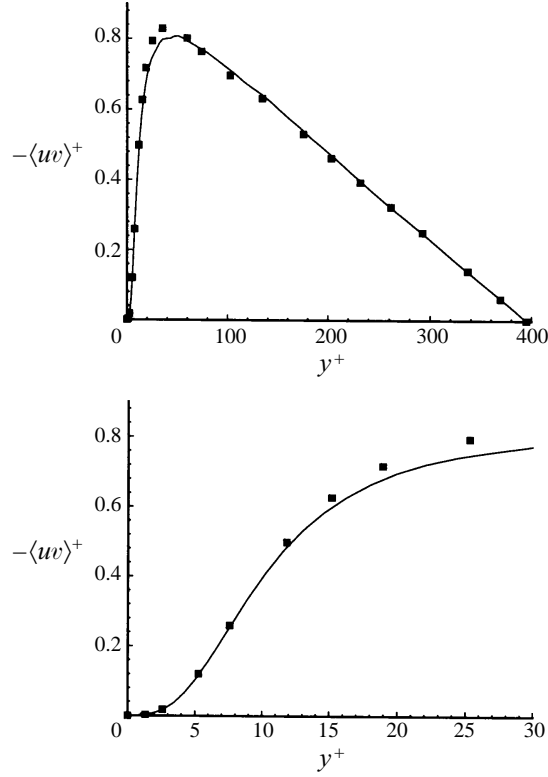


FIGURE 9. Reynolds shear stress: non-local model (line) and DNS data (symbols) for fully developed channel flow.

half-plane mean velocity changes by 2% under a grid refinement to 90 cells. Particle velocities, normalized by the friction velocity, are shown in figure 7. Mean quantities are computed using the non-parametric regression of Dreeben & Pope (1992) of the particle results, which is described in the Appendix, §A.2. Mean quantity calculations are repeated and time averaged over a stationary numerical solution to the stochastic differential equations. This produces the mean velocity profile of figure 8 from the particle results of figure 7. Mean velocity with the non-local model shows improved agreement over the local model profile of figure 3(a), because the Reynolds shear stress of figure 9 is correct very close to the wall, although the peak shear stress is slightly underpredicted. The near-wall suppression of v' by (4.16) and the boundary condition (4.15) is shown in figure 10. Fluctuating velocities are determined by taking each particle velocity and subtracting the mean velocity interpolated at the particle's location. Streamwise and wall-normal fluctuations appear in figure 10 on the same scale to show their relative magnitudes. Comparison of the near-wall scaling of k and $\langle uv \rangle$ with their behaviours predicted by (4.27) and (4.30) are shown in figure 11. Only a slight discrepancy occurs within $y^+ = 2$ due to the difficulty in achieving such accuracy with the regression algorithm. As a consequence of the near-wall scaling argument, we also expect the turbulence to reach its two-component state at the wall. The anisotropy map of figure 14 verifies that this is the case, although the model and the DNS do not reach the same two-component states. Presumably this is because the model makes $\langle v^2 \rangle$ scale like y^3 while the correct physical behaviour is to scale like y^4 . Other comparisons of model results with DNS are shown in

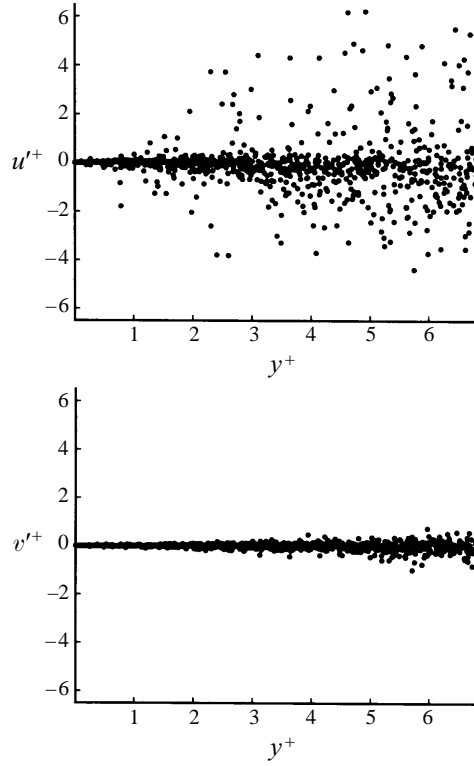


FIGURE 10. Particle fluctuating velocities for the non-local model.

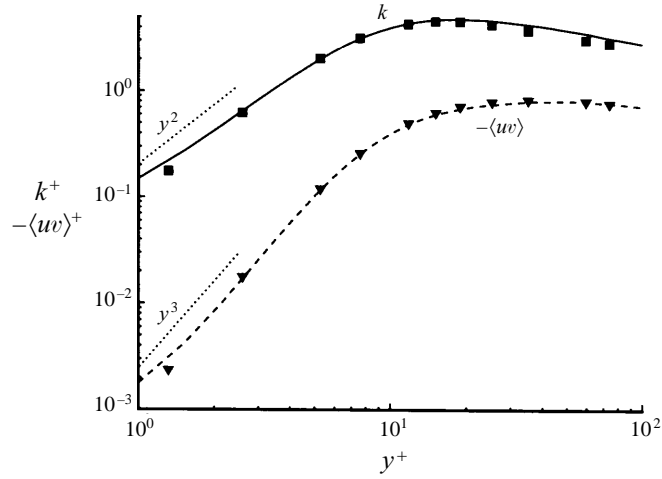


FIGURE 11. Near-wall scaling of kinetic energy and Reynolds shear stress for fully developed channel flow: comparison of the non-local model (line) with DNS data (symbols).

figures 13–16. In the budgets of $\langle u^2 \rangle$ and $\langle uv \rangle$ shown in figure 15, T_v is viscous transport, T_T is turbulent transport (triple correlation), P is production, ϕ is the correlation of fluctuating velocity and pressure gradients, and ϵ is the dissipation. The differences of the fluctuating pressure and dissipation terms are shown together, because the generalized Langevin model does not distinguish them in (3.7). Also,

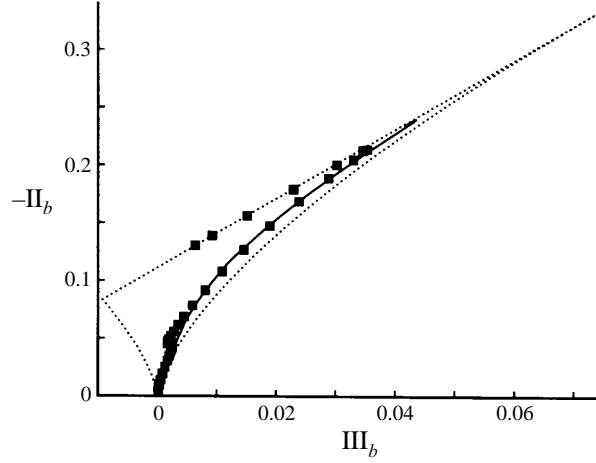


FIGURE 12. Anisotropy map: non-local model (line) and DNS data (symbols) for fully developed channel flow.

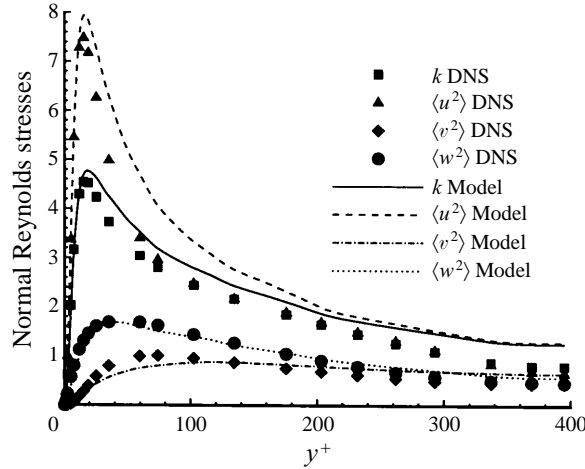


FIGURE 13. Normal Reynolds stresses: non-local model (line) and DNS data (symbols) for fully developed channel flow

turbulent transport terms are not computed directly because the statistical error associated with triple moments is too severe for the regression algorithm. Instead, we take the transport to be the negative sum of the remaining terms, which is valid for the stationary solution.

The most significant difficulty for the p.d.f. model occurs in the ratio of production to dissipation in figure 16. A key assumption for near-wall turbulence models is that the turbulent transport can be neglected in the logarithmic layer (in this case from $y^+ = 40$ to about 120), and that the production equals the dissipation there. While the DNS bears this out, the p.d.f. model does not, even though the turbulent transport appears in (3.7) in closed form. The corresponding departure of the turbulent transport term from zero can be seen in the budget of $\langle u^2 \rangle$ shown in figure 15(a). The turbulent transport is modelled with the p.d.f. method primarily through the

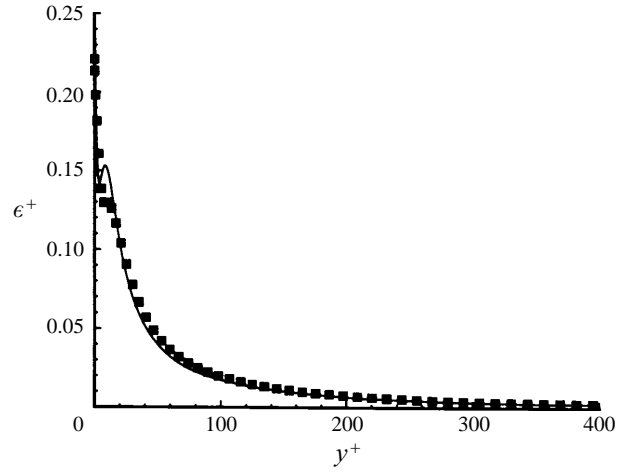


FIGURE 14. Dissipation: non-local model (line) and DNS data (symbols) for fully developed channel flow

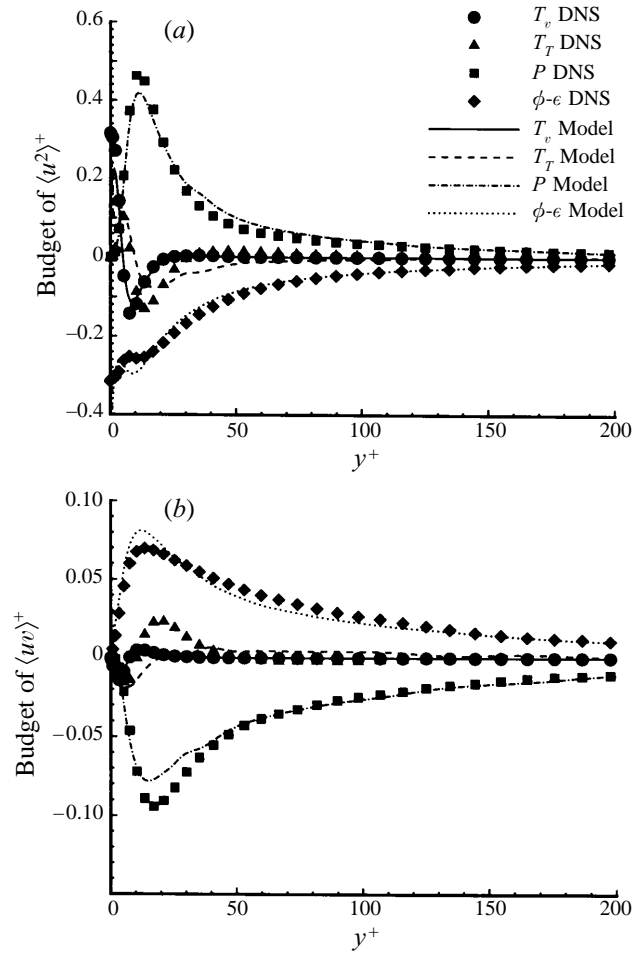


FIGURE 15. Budget of (a) $\langle u^2 \rangle$ and (b) $\langle uw \rangle$ for fully developed channel flow: comparison of the non-local model (line) with DNS data (symbols).

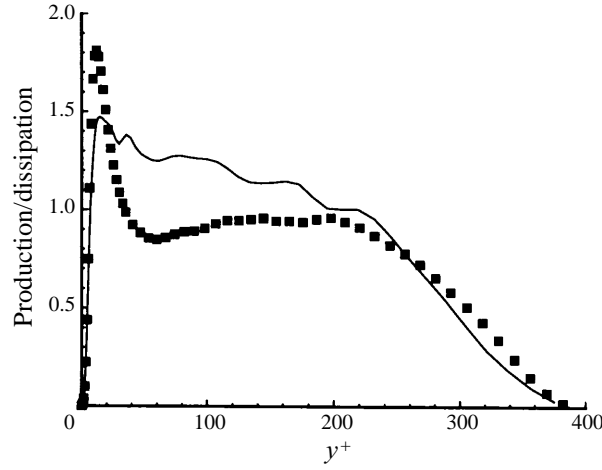


FIGURE 16. Production/dissipation for fully developed channel flow: comparison of the non-local p.d.f. model (solid line) with DNS data (symbols).

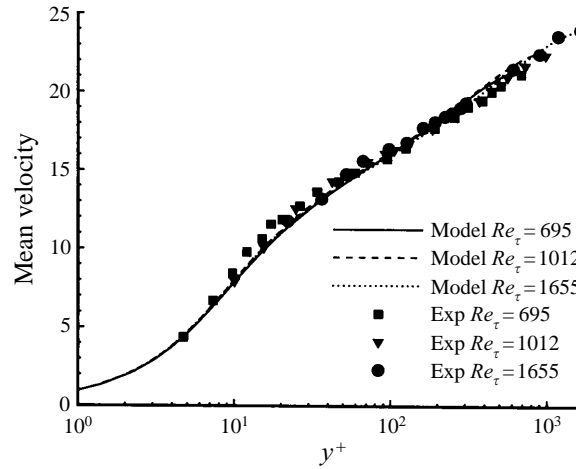


FIGURE 17. Mean velocity for fully developed channel flow: comparison of the non-local model (line) with data of Wei & Willmarth (symbols) at different Reynolds numbers.

generalized Langevin model (see Pope 1993b). Ultimately this can be corrected either by revisiting the generalized Langevin model with the transport in mind, or through compensation with the ω model. Low values of the von Kármán constant between $\kappa = 0.30$ and 0.32 are found in figure 17.

Model velocity profiles and friction coefficient over varying Reynolds numbers are shown in figures 17 and 18. For each case, the chosen number of grid cells increases with the Reynolds number. The velocity profiles are compared to the experimental channel flow data of Wei & Willmarth at Reynolds numbers $Re_h = 14\,914$, $22\,776$, and $39\,582$, with Re_h based on the mean velocity at the channel half-plane and on the channel half-width. Based on previous work of Dreeben & Pope (1997a), these correspond to $Re_\tau = 695$, 1012 , and 1655 respectively. Model results for the friction coefficient are compared with the experimental data compiled by Dean (1978). For half-plane mean velocity $\langle U \rangle_h$, the friction coefficient $C_f = \tau_w / (\frac{1}{2} \rho \langle U \rangle_h^2)$, is plotted

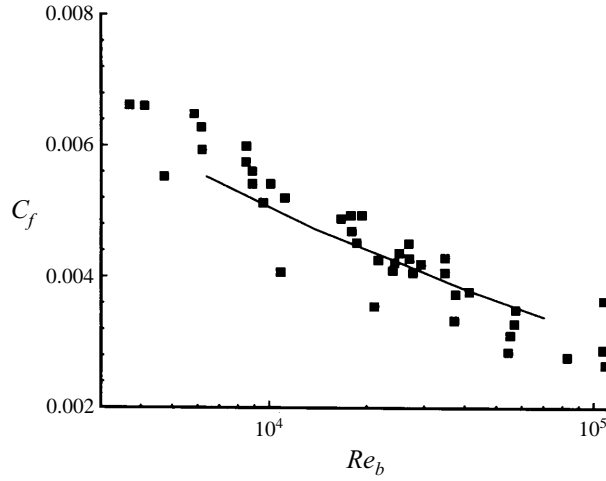


FIGURE 18. Friction coefficient as a function of Reynolds number for fully developed channel flow: comparison of the non-local model (line) with data compiled by Dean

against the Reynolds number Re_b , based on the bulk mean velocity and the full channel width.

6. Conclusion

Near-wall modelling capability is now included in the p.d.f. method. Two central aspects of the model enable adequate representation down to the wall. First, Brownian motion of the particles allows the terms involving viscous transport to be represented in the equations in closed form. This feature allows imposition of the no-slip and impermeability conditions on particles. Second, elliptic relaxation in the generalized Langevin model is used to implement an analogy to the fluctuating continuity equation close to the wall. This enables adequate representation of the near-wall anisotropy. Comparison of a p.d.f./Monte Carlo simulation with DNS and experimental results demonstrates the viability of the model.

It is always a virtue for a turbulence model to extend to as many different sorts of flows as possible beyond those for which it has been tested and beyond those for which data can be made available. The weakest link in the ability of this model to extend its validity is in the model for ω . This is partly because the ω model is still under development with the p.d.f. method. Like the ϵ equation throughout its development, the ω model incorporates modifications for different flow situations. The current model is no exception: the term involving $(P/\epsilon)^3$ in (4.13) is chosen to correct an underprediction of the mean velocity near the channel half-plane, based on DNS data for only channel flow; and in the velocity model, the term of (4.10) was implemented by Dreeben & Pope (1997a) to improve the model's performance on the logarithmic region. As a result, extension of this model to other flows cannot be taken for granted. However, two central aspects of the model which do extend are the representation of inhomogeneity and near-wall anisotropy. The appearance of viscous transport terms in closed form is clearly valid for any turbulent flow, and the analysis of the near-wall scaling of the Reynolds stresses based on the suppression of v' also applies to any wall-bounded flow. The ability of elliptic relaxation to extend to a broad class of turbulent flows is not yet established, but promising results have been

achieved with the $k-\epsilon-v^2$ model of Durbin (1995) for separated flows. While the need to model more complex flows may necessitate changes to the non-local model, the arguments developed here for the treatment of near-wall inhomogeneity, anisotropy, and boundary conditions are sufficiently sound that their formulation can plausibly remain in p.d.f. treatments which extend to the wall.

We wish to thank Professor David Ruppert for his useful discussions with us on the subject of non-parametric regression. This work was supported by AFOSR award F49620-93-1-0316.

Appendix. Numerical issues

A.1 Unbounded coefficients of the governing equations

As $y \rightarrow 0$, the quantity G_{ij} in the linear drift term of (3.3) becomes negative without bound. This is clear from (4.5) and the boundary conditions imposed on k in §3: as the wall is approached,

$$G_{ij} \sim \frac{-\epsilon}{2k} \delta_{ij} \sim \frac{-1}{y^2} \delta_{ij}, \quad (\text{A } 1)$$

and from the no-slip condition on velocities,

$$(\mathcal{U}_j - \langle U_j \rangle) \sim y. \quad (\text{A } 2)$$

So the combined term scales with $1/y$, and it becomes unbounded as $y \rightarrow 0$. Special numerical treatment is required to handle this term.

To show how the numerics need to be modified, we solve an ordinary differential equation with the same difficulty as the one described above. For coefficients a and b which are independent of time, consider the initial value problem

$$dU = a dt + bU dt, \quad (\text{A } 3)$$

$$U(0) = U_0. \quad (\text{A } 4)$$

Of the many methods available for solving this, one which provides the best analogy for the numerical solution of (3.3) is to put the linear term of (A 3) on the left-hand side, multiply through by the integrating factor e^{-bt} , and then solve for $U(t) - U_0$:

$$U(t) - U_0 = a \int_0^t e^{b(t-s)} ds + (e^{bt} - 1) U_0. \quad (\text{A } 5)$$

Now consider two different approaches for the numerical solution of (A 3) over a finite time step Δt . The first is to replace dt with Δt in (A 3), and use the known coefficients and U at $t = 0$ to approximate $U(\Delta t)$. The second is to replace t with Δt in (A 5), and use that to determine $U(\Delta t)$. Clearly the first method has a restriction that

$$\Delta t < \frac{\text{constant}}{|b|} \quad (\text{A } 6)$$

in order to achieve a stable solution; the second method has no such restriction. The relevant case to consider is, what happens as $b \rightarrow -\infty$? In that limit, the increment of U in the first method becomes undefined for any non-zero Δt , but the increment in the second method, based on the analytical solution, is defined and well behaved. The numerical scheme for (3.3) is based on this second approach to the solution of (A 3).

Equation (3.3) is a vector stochastic differential equation of the form

$$d\mathbf{U} = \mathbf{A}dt + \mathbf{B} \mathbf{U}dt + C d\mathbf{W}(t). \quad (\text{A } 7)$$

This equation is more complicated than (A 3) in two respects. First it is a vector equation with coefficients \mathbf{A} , \mathbf{B} , and C taken as a vector, a matrix, and a scalar respectively. Second, it includes the stochastic term $C d\mathbf{W}(t)$. But the problem associated with the unbounded coefficient is identical to that of (A 3): here we have

$$\lim_{y \rightarrow 0} \det [\mathbf{B}] = -\infty. \quad (\text{A } 8)$$

For coefficients \mathbf{A} , \mathbf{B} , and C frozen over the time step Δt , we use the matrix exponential integrating factor

$$e^{-\mathbf{B}t} \quad (\text{A } 9)$$

to obtain the analytical solution to (A 7)

$$\mathbf{U}(\Delta t) - \mathbf{U}_0 = \int_0^{\Delta t} e^{\mathbf{B}(\Delta t-s)} \mathbf{A} ds + (e^{\mathbf{B}\Delta t} - \mathbf{I}) \mathbf{U}_0 + \int_0^{\Delta t} C e^{\mathbf{B}(\Delta t-s)} d\mathbf{W}(s), \quad (\text{A } 10)$$

where the stochastic integral on the right-hand side is the Ito integral (see Bhattacharya & Waymire 1990; Gardiner 1990). This integral is taken as the sum of infinitesimal Gaussian random vectors; the result is a Gaussian random vector with covariance matrix

$$\int_0^{\Delta t} e^{(\mathbf{B} + \mathbf{B}^T)(\Delta t-s)} ds. \quad (\text{A } 11)$$

We now have an expression for the increment of \mathbf{U} in terms of integrals of the matrix exponential, all of which are defined and well-behaved in the limit as $\det [\mathbf{B}] \rightarrow -\infty$. These expressions are computed using the methods of Van Loan (1978).

A.2 Estimation of turbulent statistics and their gradients

The p.d.f. model developed here relies on the use of mean turbulent quantities and their first and second spatial derivatives, based on the ensemble of particle properties. Mean quantities such as $\langle u_i u_j \rangle$ and $\langle \omega \rangle$ are used in the coefficients of the particle equations (2.13), (3.3), and in the forcing terms of the elliptic relaxation equations (4.8). A two-stage non-parametric regression method of Dreeben & Pope (1992) is used to estimate the mean quantities from the particle properties. In this method, kernel estimates of Priestly & Chao (1972) are formed from the particle properties and evaluated at the centres of mass of the kernels. The linear least-squares algorithm of Ruppert & Wand (1994) is then used locally on these kernel estimates to provide final estimates at the grid nodes. Mean quantities at the particle locations are formed by linear interpolation of the nodal estimates.

For the current near-wall model, the two-stage method is extended because velocity gradients are needed in the source term of (4.8), and the second derivative of velocity is needed for the viscous term of (3.3). For first derivatives, central differences of the kernel estimates on the grid are evaluated at the centres of mass and used in the local least-squares algorithm. For second derivatives, five-point second differences of the kernel estimates (chosen to minimize statistical error) are used in the local least-squares algorithm.

REFERENCES

- BHATTACHARYA, R. N. & WAYMIRE, E. C. 1990 *Stochastic Processes with Applications*. Wiley.
- COLUCCI, P. J., JABERI, F. A., GIVI, P. & POPE, S. B. 1998 The filtered density function for large eddy simulation of turbulent reacting flows. *Phys. Fluids*, to be submitted.
- CRAFT, T. J. & LAUNDER, B. E. 1995 Improvements in near-wall reynolds-stress modelling for complex flow geometries. In *Tenth Symposium on Turbulent Shear Flows, University Park, PA*.
- DALY, B. J. & HARLOW, F. H. 1970 Transport equations of turbulence. *Phys. Fluids* **13**, 2634–2649.
- DEAN, R. B. 1978 Reynolds number dependence of skin friction and other bulk flow variables in two-dimensional rectangular duct flow. *Trans. ASME: J. Fluids Engng* **100**, 215–223.
- DELARUE, B. J. & POPE, S. B. 1997 Application of PDF methods to compressible turbulent flows. *Phys. Fluids* **9**, 2704–2715.
- DEMUREN, A. O. & WILSON, R. V. 1994 On elliptic relaxation near wall models. In *Transition, Turbulence and Combustion*, Vol. II, pp. 61–71. Kluwer.
- DREEBEN, T. D. 1996 Pdf modeling of near-wall turbulent flows. PhD thesis, Cornell University, Ithaca, NY.
- DREEBEN, T. D. & POPE, S. B. 1992 Nonparametric estimation of mean fields with application to particle methods for turbulent flows. *Tech. Rep. FDA-92-13*. Cornell University, Ithaca, N.Y.
- DREEBEN, T. D. & POPE, S. B. 1997a Pdf and Reynolds-stress modeling of near-wall turbulent flows. *Phys. Fluids* **9**, 154–163.
- DREEBEN, T. D. & POPE, S. B. 1997b Wall-function treatment in Pdf methods for turbulent flows. *Phys. Fluids* **9**, 2692–2703.
- DURBIN, P. A. 1991 Near-wall turbulence closure modeling without ‘damping functions’. *Theor. Comput. Fluid Dyn.* **3**, 1–13.
- DURBIN, P. A. 1993 A Reynolds-stress model for near-wall turbulence. *J. Fluid Mech.* **249**, 465–498.
- DURBIN, P. A. 1995 Separated flow computations with the $k-\epsilon-v^2$ model. *AIAA J.* **33**, 659–664.
- EINSTEIN, A. 1926 *Investigations on the Theory of the Brownian Movement*. Methuen and Co. Ltd. Translation by A. D. Cowper (ed. R. Furth).
- GARDINER, C. W. 1990 *Handbook of Stochastic Methods for Physics, Chemistry and the Natural Sciences*, 2nd edn. Springer.
- HANJALIC, K. & LAUNDER, B. E. 1976 Contribution towards a Reynolds-stress closure for low-Reynolds-number turbulence. *J. Fluid Mech.* **74**, 593–610.
- HAWORTH, D. C. & POPE, S. B. 1986 A generalized Langevin model for turbulent flows. *Phys. Fluids A* **29**, 387–405.
- HAWORTH, D. C. & POPE, S. B. 1987 A Pdf modeling study of self-similar turbulent free shear flows. *Phys. Fluids A* **30**, 1026–1044.
- JAYESH & POPE, S. B. 1995 Stochastic model for turbulent frequency. *Tech. Rep. FDA-95-05*. Cornell University, Ithaca, NY.
- KARATZAS, I. & SHREVE, S. E. 1991 *Brownian Motion and Stochastic Calculus*, 2 edn, Springer.
- KOLMOGOROV, A. N. 1941 The local structure of turbulence in incompressible viscous fluid for very large Reynolds numbers. *Dokl. Akad. Nauk SSSR* **32**, 19–21.
- LAI, Y. G. & SO, R. M. C. 1990 On near-wall turbulent flow modelling. *J. Fluid Mech.* **221**, 641–673.
- LAUNDER, B. E., REECE, G. J. & RODI, W. 1975 Progress in the development of a Reynolds-stress turbulence closure. *J. Fluid Mech.* **68**, 537–566.
- LAUNDER, B. E. & SPALDING, D. B. 1974 The numerical computation of turbulent flows. *Comput. Meth. Appl. Mech. Engng* **3**, 269–289.
- LAUNDER, B. E. & TSELEPIDAKES, D. P. 1991 Progress and paradoxes in modelling near-wall turbulence. In *Eighth Symposium on Turbulent Shear Flows*, Munich, Germany.
- LAURENCE, D., DURBIN, P. & DEMUREN, A. O. 1995 Modelling near-wall effects in second moment closures by elliptic relaxation. In *Tenth Symposium on Turbulent Shear Flows, University Park, PA*.
- LUMLEY, J. L. 1978 Computational modeling of turbulent flows. *Adv. Appl. Mech.* **18**, 123–176.
- MANSOUR, N. N., KIM, J. & MOIN, P. 1988 Reynolds-stress and dissipation-rate budgets in a turbulent channel flow. *J. Fluid Mech.* **194**, 15–44.
- NAOT, D., SHAVIT, A. & WOLFSHTEIN, M. 1970 Interactions between components of the turbulent velocity correlation tensor. *Israel J. Tech.* **8**, 259–269.

- NORRIS, A. T. & POPE, S. B. 1995 Modeling of extinction in turbulent diffusion flames by the velocity-dissipation-composition PDF method. *Combust. Flame* **100**, 211–220.
- POPE, S. B. 1985 Pdf methods for turbulent reactive flows. *Prog. Energy Combust. Sci.* **11**, 119–192.
- POPE, S. B. 1991 Application of the velocity-dissipation probability density function model to inhomogeneous flows. *Phys. Fluids A* **3**, 1947–1957.
- POPE, S. B. 1993a Boundary treatment in the stochastic Lagrangian wall model. Unpublished.
- POPE, S. B. 1993b On the relationship between stochastic-Lagrangian models of turbulence and second-moment closures. *Phys. Fluids* **6**, 973–985.
- POPE, S. B. 1994a Lagrangian PDF methods for turbulent flows. *Ann. Rev. Fluid Mech.* **26**, 23–63.
- POPE, S. B. 1994b PDF2DV. A Fortran code to solve the modelled joint PDF equations for two-dimensional recirculating flows. Unpublished.
- POPE, S. B. & CHEN, Y. L. 1990 The velocity-dissipation probability density function model for turbulent flows. *Phys. Fluids A* **2**, 1437–1449.
- PRIESTLY, M. B. & CHAO, M. T. 1972 Non-parametric function fitting. *J. R. Statist. Soc.* **34**, 385–392.
- RODI, W. 1980 *Turbulence Models and Their Application in Hydraulics - a State of the Art Review*. Intl Assoc. for Hydraulic Research.
- ROTTA, J. C. 1951 Statistische theorie nichthomogener turbulenz. *Z. Physik* **129**, 547–572.
- RUPPERT, D. & WAND, M. P. 1994 Multivariate locally weighted least squares regression. *Ann. Statist.* **22**, 1346–1370.
- SAXENA, V. & POPE, S. B. 1996 PDF calculations of non-premixed methane flames with detailed chemistry. In *Combustion Institute - Eastern States' Fall Technical meeting, Hilton Head, SC*.
- SHIH, T. S. & LUMLEY, J. L. 1993 Kolmogorov behavior of near-wall turbulence and its application in turbulence modeling. *Intl J. Comput. Fluid Dyn.* **1**(1), 43–56.
- SINGHAL, A. K. & SPALDING, D. B. 1981 Predictions of two-dimensional boundary layers with the aid of the $k-\epsilon$ model of turbulence. *Comput. Meth. Appl. Mech. Engng* **25**, 365–383.
- SO, R. M. C., LAI, Y. G. & ZHANG, H. S. 1991 Second-order near-wall turbulence closures: A review. *AIAA J.* **29**, 1819–1835.
- SPALDING, D. B. 1977 *GENMIX - A General Computer Program for Two-Dimensional Parabolic Phenomena*. Pergamon.
- SUBRAMANIAM, S. & POPE, S. B. 1997 Comparison of model predictions for the periodic reaction zone model problem. *Tech. Rep.* Cornell University, Ithaca, NY.
- VAN DRIEST, E. R. 1956 On turbulent flow near a wall. *J. Aero. Sci.* **23**, 1007–1011.
- VAN LOAN, C. F. 1978 Computing integrals involving the matrix exponential. *IEEE Trans. on Automatic Control* **ac-23**, 395–404.
- VAN SLOOTEN, P. R., JAYESH & POPE, S. B. 1998 Advances in PDF modeling for inhomogeneous turbulent flows. *Phys. Fluids*, submitted.
- WAX, N. 1954 *Noise and Stochastic Processes*. Dover.
- WEI, T. & WILLMARTH, W. W. 1989 Reynolds-number effects on the structure of a turbulent channel flow. *J. Fluid Mech.* **204**, 57–95.
- WILCOX, D. C. 1993 *Turbulence Modeling for CFD*. DCW Industries.
- WOELFERT, A. 1995 PDF-simulation of turbulent channel flow including near-wall sublayer using a generalized Langevin model. *Tech. Rep.* 95-33, Heidelberg University.
- YEUNG, P. K. & POPE, S. B. 1989 Lagrangian statistics from direct numerical simulations of isotropic turbulence. *J. Fluid Mech.* **207**, 531–586.